

Possible origin of the spatiotemporal evolution of the 2008 earthquake swarm in Northwest-Bohemia, Czech Republic

Jens Heinicke ^{a,*}, Thomas Braun ^b, Catherine Alexandrakis-Zieger ^a, Stefan Buske ^a

^a Institute of Geophysics and GeoInformatics, TU Bergakademie Freiberg, Gustav-Zeuner-Str. 12, 09599 Freiberg, Germany

^b Istituto Nazionale di Geofisica e Vulcanologia, Roma1, Osservatorio Sismologico Arezzo, Via F. Redi, 13, 52100 Arezzo, Italy



ARTICLE INFO

Keywords:
 Seismotectonics
 Induced seismicity
 Earthquake swarm
 Pore pressure diffusion
 NW-Bohemia

ABSTRACT

The phenomenon 'earthquake swarm' is well known from numerous locations on Earth but its mechanism and trigger process are still an enigma. The influence of fluids on fluid-driven seismicity is generally well accepted but the temporal behaviour and the migration of activated phases is still an open question. We attempt to answer these open questions by combining the results of research on induced-seismicity with new reliable analyses of full moment tensors (FMTs) of the swarm earthquakes of 2008 to 2018 in Northwest-Bohemia, Czech Republic by Vavryčuk et al. (2017, 2021). The FMTs reveal evidence of compressive fracturing as the prevailing focal mechanism during the swarms. Our proposed hypotheses considered these earthquakes as the origin of subsequent pore pressure pulses in the respective active swarm phase. The diffusion of these pore pressure pulses, which could trigger the nearby earthquakes as well as the successive swarm phase in the vicinity after a respective diffusion process in space and time, are the target of this studies. Missing information regarding the real diffusion distances are compiled by a strict statistical approach of a one-to-one analysis of the swarm earthquakes. The analyses suggest that parts of the swarm earthquakes could be triggered by pore pressure diffusion with an estimated diffusivity range of approximately $D = 0.01$ to $3.0 \text{ m}^2/\text{s}$. In exceptional cases, which make about 5% of all cases, we have to consider also diffusivities up to $15 \text{ m}^2/\text{s}$. Examples of hydraulic diffusivities observed in our region of interest confirm this range. Such a process can also be assumed during further swarms in the years 2011 to 2018 because of the continuous and predominant occurrence of compressive fracturing as a focal mechanism beside pure shear and tensile fracturing. Our results could explain for the first time the missing link regarding the temporal and spatial migration of the subsequent swarm phases in our studied region at Nový Kostel (Northwest-Bohemia, Czech Republic).

1. Introduction

Swarm earthquakes are clustered in space and time without any clear mainshock–aftershock sequence. The Coulomb failure criterion explains such earthquake clustering as initiated by pore pressure variations. Two types of driving forces of seismic swarms have been suggested: (i) fluid pressure increase due to upward migration of magma and other juvenile fluids (Foulger et al., 2004; Shelly et al., 2013) and/or (ii) stress changes associated to aseismic slip (Eyre et al., 2020; Heinicke et al., 2019; Vidale and Shearer, 2006). The local static and dynamic stress changes of the events affect the stress field and influence the self-organization of the swarm activity (Fischer and Horálek, 2005). Such stress transients show a fast decay in amplitude and therefore cannot be deemed as an explanation of the comprehensive spatiotemporal activity of the

subsequent swarm phases. In this paper, we consider a new approach, which combines the results of new moment tensor analyses by Vavryčuk and Hrbcová (2017) and the proposed fluid driven seismicity mechanism due to pore pressure perturbations and their diffusion (Parotidis et al., 2005).

The Northwest-Bohemia and the Southern Vogtland region is well known for its earthquake swarm activity that was documented for the first time in the 18th century (Dahm et al., 2018). Its typical behaviour shows space-time dependent seismicity clusters with no dominating main shock, but rather numerous low magnitude earthquakes at different activity phases over weeks or months. However, this typical spatiotemporal behaviour is still an enigma, which has been attempted to explain by different approaches (Dahm et al., 2008; Fischer et al., 2014; Hainzl and Fischer, 2002). Stress accumulation in the regional

* Corresponding author at: Institute of Geophysics and GeoInformatics, TU Bergakademie Freiberg, Gustav-Zeuner-Str. 12, 09599 Freiberg, Germany.
 E-mail address: jens.heinicke@extern.tu-freiberg.de (J. Heinicke).

stress field (Heidbach et al., 2018), alteration of the rock matrix and additional pore pressure perturbations, possibly induced by influences of the hydraulic regime, e.g. due to water level variations of the nearby Horka reservoir (Heinicke et al., 2018), are probably the main reasons for the onset of the very first single earthquakes at the beginning of earthquake swarms in the Nový Kostel focal zone.

In addition to different clusters of seismic events in the region of Northwest-Bohemia/Vogtland, the most active seismicity cluster is located around the village of Nový Kostel (NK, 12.45°E, 50.21°N, Fig. 1), concentrated in an area of approximately 10 km × 2 km, extending predominantly in the SSE-NNW direction, and at focal depths of between 7 and 12 km. The most prominent earthquake swarms (magnitude of the strongest shock in parentheses) occurred in the years 1985/86 ($M_{L\max}$ 4.6), 2000 ($M_{L\max}$ 3.2), 2008 ($M_{L\max}$ 3.8), 2011 ($M_{L\max}$ 3.5), 2014 ($M_{L\max}$ 4.2), and 2018 ($M_{L\max}$ 3.8). A comprehensive review of the geological and seismotectonic settings is presented by Fischer et al. (2014). Since the earthquake swarm of 1997 ($M_{L\max}$ 2.9), several analytical results concerning its interpretation reveal an important influence of pore fluids on the triggering process and the spatiotemporal behaviour of the seismicity (Fischer et al., 2017; Hainzl et al., 2012; Heinze et al., 2017; Horálek and Fischer, 2008; Parotidis et al., 2005). The possible influence of upwelling juvenile fluids on the local seismicity and vice versa have also been considered (Babuška et al., 2016; Bräuer et al., 2014; Bräuer et al., 2007; Weise et al., 2001). The emission of juvenile fluids, in particular CO₂, is widely distributed (Fig. 1) and fixed to local fault zones owing to their upwelling towards the surface. The isotopic signature of this magma originated CO₂ is -4 to $-2 \delta^{13}\text{C}_{\text{PDB}}$ (CO₂ (%)) and the ³He mantle contribution reaches the range of sub-continental mantle fluids (Gautheron et al., 2005) with R_a values up to 6 (Bräuer et al., 2008).

However, Heinicke et al. (2019) presented arguments for a separation between the juvenile fluids and the seismogenic clusters linked to an impermeable major fault zone (Mariánské Lázně fault zone, Fig. 1): a

mixture of juvenile and crustal fluids migrate in the western part, but only crustal fluids exist in the eastern, seismically active part. Preliminary results of our latest seismic survey provide the first evidence for a steeply dipping section of the Mariánské Lázně fault zone towards the southwest, which confirms this spatial separation (Heinicke et al., 2019). The earthquake swarm activity might therefore be triggered by various pore pressure perturbation processes including (i) fluid overpressure in general with a simultaneous reduction of the frictional strength (Hainzl et al., 2012), (ii) hydrostatic pressure increase due to hydrological events, i.e. a possible reservoir induced seismicity by the impoundment of the Horka reservoir (Heinicke et al., 2018) and/or (iii) the process of pore pressure generation, as proposed here. Nevertheless, it should be noted that the target of this study is to propose an explanation for the triggering of the different phases during a seismic swarm, and not the triggering of the initial events of the swarm itself.

Shapiro (2015) describes the one-dimensional diffusion process of pore pressure perturbations as the ‘triggering front’. The results of Parotidis et al. (2005) and Hainzl et al. (2016, 2012) reveal indications for a correlation between pore pressure perturbations and the spatiotemporal occurrence of the respective earthquake swarm phases. The estimated hydraulic diffusivities of the so-called parabolic envelope, which describe the trigger front of the earthquakes in their spatiotemporal behaviour, are in the range of 0.05 to 10 m²/s. In particular, the trigger front model by Parotidis et al. (2005) reveals an effective hydraulic diffusivity of 0.25 m²/s for the complete 2000 swarm and describes the spatiotemporal behaviour of the triggering pressure front on the base of a diffusivity dependent point-source step function. This means that the single earthquake swarm phases are always individually triggered by a new pressure point source. The nature of this pressure source is the open question. Parotidis et al. (2005) propose one possible explanation, which involves pressure perturbations by the upward migration of juvenile fluids. In the present contribution, we have modified this approach by reasonably assuming that the principal part of the swarm earthquakes could be due to a discrete and self-contained pressure point source. We propose the hypothesis that the numerous swarm earthquakes induce additional source points in the cumulative step point function probably scaled by their magnitude as a proxy of the amplitude of the pore pressure perturbation. The effect of multiple triggering fronts during their respective swarm phases could explain the general spatiotemporal behaviour of earthquake swarms in our focal zone. Arguments in favour of this approach are based on new studies of focal mechanism in the study region (Vavryčuk et al., 2021; Vavryčuk and Adamová, 2019; Vavryčuk and Hrubcová, 2017) and will be discussed in relation to the 2008 earthquake swarm.

1.1. The focal mechanisms of the 2008 earthquake swarm

We focus our investigations on the major swarm of October/November 2008. About 1000 earthquakes with precise relocated hypocentres available from the bulletin of the West Bohemia seismic network (Vavryčuk, 2021) are used for our studies. The seismological details are discussed by Fischer et al. (2010), Vavryčuk et al. (2013) and Vavryčuk and Hrubcová (2017). The relative locations of the hypocentres are of high accuracy with an uncertainty of approximately ±25 m in the horizontal plane and ± 75 m in the vertical direction (Bouchala et al., 2013; Vavryčuk et al., 2021). Bouchala et al. (2013) applied the double-difference location method and achieved the highest accuracy by using cross-correlated waveforms. Fig. 2 shows the temporal distribution of the earthquakes (magnitudes $M_L \geq 0.5$) with their 7 major phases (P1 to P7).

The most important contribution to our hypothesis derives from the analysis of full moment tensors (FMTs) from selected earthquakes of the 2008 seismic swarm. Vavryčuk and Hrubcová (2017) and Vavryčuk and Adamová (2019) analysed the FMTs of 483 swarm earthquakes and the 249 best-fit analyses were used to investigate the non-DC-components of the FMTs. The isotropic (ISO) and the compensated linear vector dipole

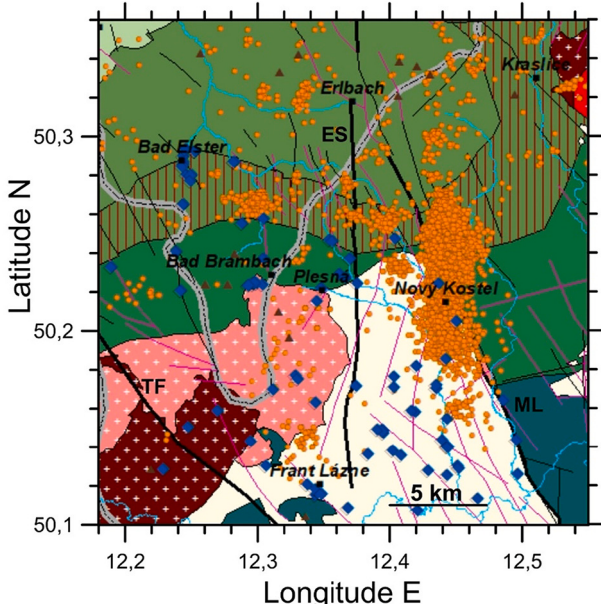


Fig. 1. Map of the study area with the main epicentral cluster at Nový Kostel: orange dots: epicentres; blue diamonds: CO₂ gas emission sites; pink/black lines: fault zones; ML: Mariánské Lázně fault zone; ES: Schönbeck – Erlbach - Skalna fault zone; TF: Tachov fault zone. Geological features: red and pink: Variscan intrusive; white: younger sediments (Cheb basin); green: different metasedimentary rocks units. Map compiled according to the geological reference maps (Cháb et al., 2007; Emmert et al., 2007; Hoth et al., 1981). (For interpretation of the references to colour in this figure legend, the reader is referred to the web version of this article.)

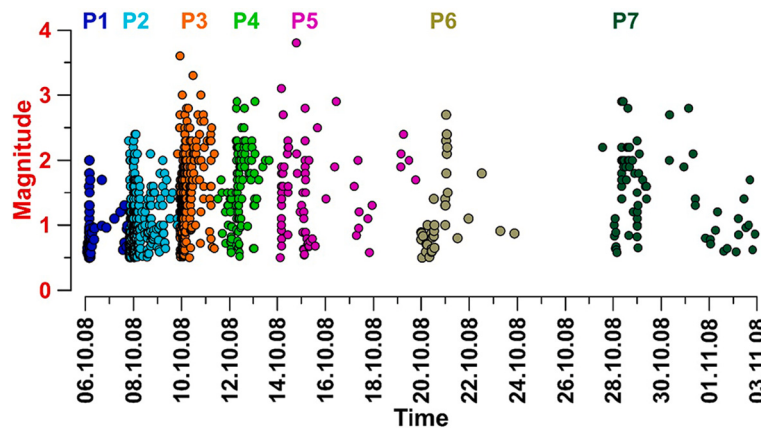


Fig. 2. The magnitude-time plot of the 2008 earthquake swarm with 7 sub-phases (P1 to P7) as coloured point clusters (local magnitudes $M_L \geq 0.5$). Bulletin according to Vavryčuk (2021).

(CLVD) components indicate seismic anisotropy and/or volumetric variations of the seismic source, i.e. the orientation of the fracturing as a tensile or compressive process (Julian et al., 1998; Vavryčuk, 2011; Vavryčuk et al., 2008; Vavryčuk, 2005). The anisotropic basement of the metamorphic rocks in our study area could have an important influence on these parameters (Vavryčuk, 1993). However, the analysis of the non-DC-components reveals well correlated ISO and CLVD values. Further, 95% of the selected events show negative CLVD and ISO components, which indicate that compressive fracturing is the predominant focal mechanism (Vavryčuk and Adamová, 2019), rather than the expected typical tensile fracturing. Vavryčuk and Hrubcová (2017) proposed this new interpretation in their fault-weakening model for the first time. The compression of fault planes occurs if the state of stress is close to critical and the fault strength has been gradually weakened to a critical value by hydrothermal alteration, e.g., due to aggressive pore fluids. Fluid-rock-interactions in the seismogenic crust depend on the high mineralization of the fluids (e.g., dissolved salts) and their acidic components (e.g., HCl, H₂SO₄) under elevated P-T conditions (Stober and Bucher, 2015; Wintsch et al., 1995). The alteration processes therefore act as an important ‘catalysator’ for the seismicity. Chen and Talwani (2001) observed a reactivation of seismicity due to the dissolution of minerals (zeolites) on zeolite-filled fracture zones and the following pore pressure diffusion along these reopened fractures, which trigger the seismicity. Our hypocentres show a collapsing of the weakened shear zone probably owing to the long-term geochemical degradation and dissolution of the wall rock. The compressive faulting can be described as a healing process, which will not be reactivated (Heinicke et al., 2009). The analysed migration of activity reveals that most events of a swarm phase occur close to the previous rupture and only a small part indicate a continuous migration.

This compressive fracturing is the key argument for our approach because it explains the collapse of the shear zone, the expulsion of the fluid phase and the generation of a new pore pressure pulse. The results of further studies by Vavryčuk et al. (2021) confirm the predominant occurrence of negative non-DC components for the swarms of the years 2011, 2014, 2017, and 2018. First indications of this process were identified for the swarms in the years 1997 (Vavryčuk, 2002) and 2000 (Horálek and Šílený, 2013) although data quality was not as excellent as today.

We combine the proposed generation of new pressure pulses with their diffusion in the open fracture zones, i.e. towards the subsequent events or swarm phase, as described in the next section. In any case, the induced pressure wave influences the local stress regime along the diffusion path and could therefore be a potential trigger of the subsequent earthquakes if the fault strength is critical enough.

2. Methods - diffusion of the triggering front

The migration of the different swarm phases can be considered in general as a diffusion process of fluid pressure pulses in the fracture zones (Hainzl et al., 2012; Parotidis et al., 2003). A simplified description of such diffusion of a 1-D pore pressure propagation front (Hainzl et al., 2012; Shapiro, 2015; Shapiro et al., 1997) can be presented for an incompressible, isotropic and homogeneous medium by eq. (1):

$$r = \sqrt{4 \pi D_{\text{eff}} t_d} \quad (1)$$

The pore pressure pulse propagates along the distance r within the diffusion time t_d according to the effective hydraulic diffusivity D_{eff} (in m^2/s). The parabolic envelope of this equation can describe the spatiotemporal expansion of the swarm phases in a r - t diagram and is an indication for a possible fluid driven process (Hainzl et al., 2012; Parotidis et al., 2005; Shapiro, 2015). A typical range of hydraulic diffusivities in the upper crust vary from $0.01 \text{ m}^2/\text{s}$ (Shapiro, 2015) and up to $10 \text{ m}^2/\text{s}$ (Talwani et al., 2007).

In our study, we investigate the pore pressure variations from the perspective of their spatiotemporal behaviour. This means, the diffusion of a new pressure wave starts from the generation of a seismically induced hydraulic pore pressure pulse (SIPPP) owing to the compressive fracturing in the respective hypocentres. The gradual variation of additional pressure pulses can be described as the algebraic sum of positive and negative terms of a step function as shown by previous investigations on induced seismicity (Costain, 2008; Durá-Gómez and Talwani, 2010; Heinicke et al., 2018; Talwani et al., 2007) leading to a superposition of relative pressure variations ($d p_i$) of an arbitrary parameter (dimensionless) at any diffusion distances r after i time steps:

$$d p_i = \sum_{k=2}^i (Q_k - Q_{k-1}) \operatorname{erfc} \left[r / \sqrt{4 D_{\text{eff}} (t_i - t_k)} \right] \quad (2)$$

where erfc is the complementary error function. Running index k marks the respective date with fixed increment time steps of the time series t in seconds. Q denotes the magnitudes of the respective earthquakes, which we use as proxy for the calculation of the amplitude of the induced pressure perturbation. For our calculations, we use a time step of 60 s and only one earthquake as a proxy for the calculation of the amplitude of the induced pressure perturbation. Because of the large number of earthquakes during a swarm phase, we select only the events with the highest magnitude per minute for our calculation. The variations of the parameter Q reveal the amplitude of the induced pressure perturbation. For example, the magnitudes of the earthquakes could be used here because they indicate as proxy the collapsed fracture area and hence the induced pressure pulse amplitude. For our studies, we apply a uniform magnitude of $M = 1$ because we study only the temporal pressure

variations in a distance r and not the amplitude. The equation states that the diffused relative pore pressure variations could generate a pore pressure front at distance r after the necessary diffusion time, which leads to fluctuations of the hydrostatic pore pressure. The episodes of increasing pore pressure destabilize the fractures and reduce the effective normal traction on fractures, such that pore pressure front acts as a seismic trigger front, bringing the fault closer to failure and triggering an earthquake, if the state of stress is close to ‘critical’.

Such SIPPPs act in addition to the hydrostatic pressure. The amplitudes of the SIPPPs are given in relative units because the real values of pressure increases are unknown. However, the amplitudes depend on the pore volume of the compressed shear plane, which is linked to the seismic moment, and hence, to the magnitude. According to Michálek and Fischer (2013) and Kolář et al. (2011), the rupture radii of the shear planes increase, from approximately 40 m for events with $M_L = 1$, to approximately 600 m for events with $M_L = 3.8$, during the 2008 earthquake swarm. The temporal delay as trigger of the subsequent phase and the typical attenuation of the SIPPP depend on the effective diffusivity along the diffusion path (fracture zones) such that the trigger fronts disappear after the respective distance and time.

2.1. Two examples of trigger fronts

For the evaluation of our hypothesis, we consider only a simplified model with a single pressure front associated with one earthquake as pressure source because of the missing data of the real processes. In other words, we reduce the analysis to the given data set so that we assume the diffusion time (temporal difference between two events of successive swarm phases) and the diffusion distance between these pairs of events to consider this process as a one-to-one trigger mechanism.

The diffusion of the SIPPPs occurs in all directions along an interconnected fracture system starting from the hypocentre, whereby we have to assume a heterogeneity of the hydraulic diffusivity along the fractures. Therefore, we estimate the diffusivity as an effective value over time and respective diffusion paths. The diffusion paths are calculated as the direct distance from the hypocentre of our pressure source to the successive events.

To demonstrate the behaviour of a single trigger front, Figs. 3 and 4 show the spatiotemporal behaviour of a SIPPP induced by a single earthquake of magnitude $M = 1$ for two exemplary diffusion distances: $\Delta s = 500$ m (Fig. 3) and $\Delta s = 1000$ m (Fig. 4) and different hydraulic

diffusivities (0.08, 0.1, 0.3, 0.5, 0.7, and $1.0 \text{ m}^2/\text{s}$), respectively. The period of increasing pore pressure indicated by horizontal bars according to their diffusivity is relevant for triggering the earthquakes in the subsequent swarm phase in the respective distance. We use in our analysis these temporal fix points: T_{\min} for the starting point of the pore pressure increase and T_{\max} for their termination. Furthermore, the introduction of two ‘hypothetical’ seismic events represents the possible trigger process, which occurred at the presented distances of $\Delta s = 500$ m (brown star in Fig. 3) and of $\Delta s = 1000$ m (blue star in Fig. 4). The most part of the SIPPP-graphs, characterized by different diffusivities, indicate that an increasing pore pressure trend could be able to trigger the hypothetical events. It is impossible to evaluate which diffusivity would be the most realistic, but we can approximate the relevant diffusivity range. Fig. 3 suggests a diffusivity range of $D = 0.1$ to $0.3 \text{ m}^2/\text{s}$, whereby the diffusivity could be even smaller than $0.1 \text{ m}^2/\text{s}$ but in this case the amplitude of the relative pressure variations would decrease significantly. Fig. 4 implies a diffusivity range of $D = 0.3$ to $1.0 \text{ m}^2/\text{s}$. The diffusivities of $D \geq 0.3 \text{ m}^2/\text{s}$ in Fig. 3 and of $D \geq 1.0 \text{ m}^2/\text{s}$ in Fig. 4 mark the maximum diffusivities for those exemplary diffusion distances, otherwise the pressure wave becomes too fast and would diminish before an event could be triggered. We apply this exemplary analysis of the proposed events (brown and blue stars) with respect to the parameter T_{\max} in Figs. 5 and 6.

To analyse the spatiotemporal behaviour of the SIPPPs, we considered a wider range of diffusivities, from $D = 0.1$ to $2.0 \text{ m}^2/\text{s}$. We calculated numerous examples of T_{\max} , by varying diffusion distances r , diffusion times t , and diffusivities D and obtained a catalogue of periods with increased pore pressure, which can be applied to different spatiotemporal conditions. Fig. 5 illustrates the possibility of whether an earthquake could be triggered by a SIPPP (with the respective D) after a certain delay (t) and distance (r) with respect to the preceding event. The figure shows the distribution of the calculated T_{\max} as r - t - D plot for an exemplary diffusivity of $D = 0.7 \text{ m}^2/\text{s}$ according to the respective pore pressure variations. T_{\min} stands for the minimum periods, which are necessary for the approach of the pressure waves in the respective diffusion distances and T_{\max} indicates the upper temporal limit of pressure increase with respect to the respective diffusivity range. The graph of the exemplary diffusivity of $D = 0.7 \text{ m}^2/\text{s}$ is the result of the calculated pressure waves in the respective distances indicated by black lines in Fig. 5. The ‘hypothetical’ events in the Figs. 3 and 4 are also indicated - only the blue one could be triggered by this exemplary SIPPP

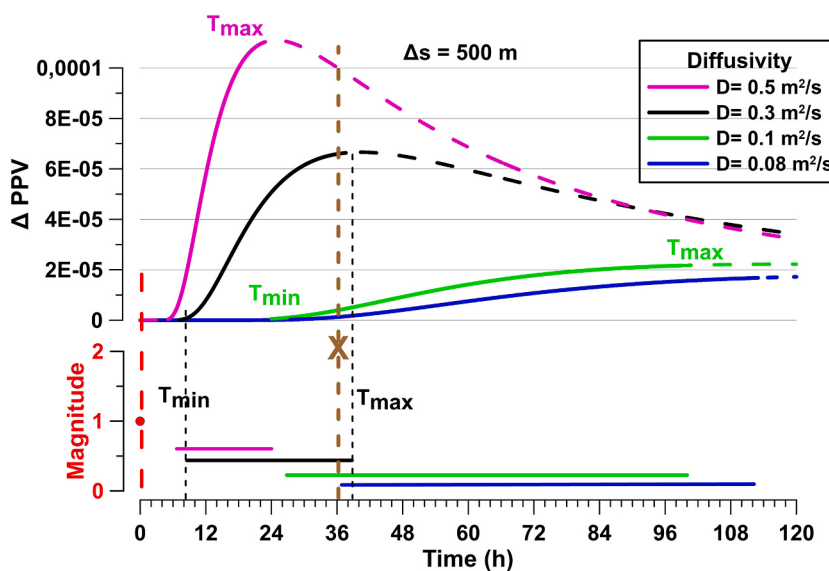


Fig. 3. Spatiotemporal behaviour of the relative pore-fluid pressure variations (ΔPPV) induced by an earthquake with a compressive shear process. The diffusion distance is assumed with $\Delta s = 500$ m. The calculated SIPPPs are displayed with different hydraulic diffusivities (coloured lines, see legend). The amplitude of the relative ΔPPV depends on the amplitude of the proxy parameter, in our case the magnitude of the earthquake (e.g., $M = 1$, red point). Periods of increasing pore pressure could be relevant to trigger subsequent events. Such periods are indicated by solid lines and horizontal bars above the x-axis according to their diffusivity. The horizontal bars also mark the starting point (T_{\min}) and the termination of this period (T_{\max}). Dashed lines indicate the periods without pressure increase and no trigger effect. Additionally, ‘hypothetical’ triggered event, is shown in the figure as brown star (magnitude is not relevant). The event occurred 36 h after the assumed pressure pulse starts to diffuse. It is important to note that not all SIPPPs could have triggered this event because of the decreasing amplitude of the pore pressure front if $D > 0.3 \text{ m}^2/\text{s}$ or the probably very low amplitude of pressure increase (e.g., $D \leq 0.08 \text{ m}^2/\text{s}$). However, we are unable to resolve which diffusivity would be the real one but its range can be approximated: probably between 0.1 and $0.3 \text{ m}^2/\text{s}$. (For interpretation of the references to colour in this figure legend, the reader is referred to the web version of this article.)

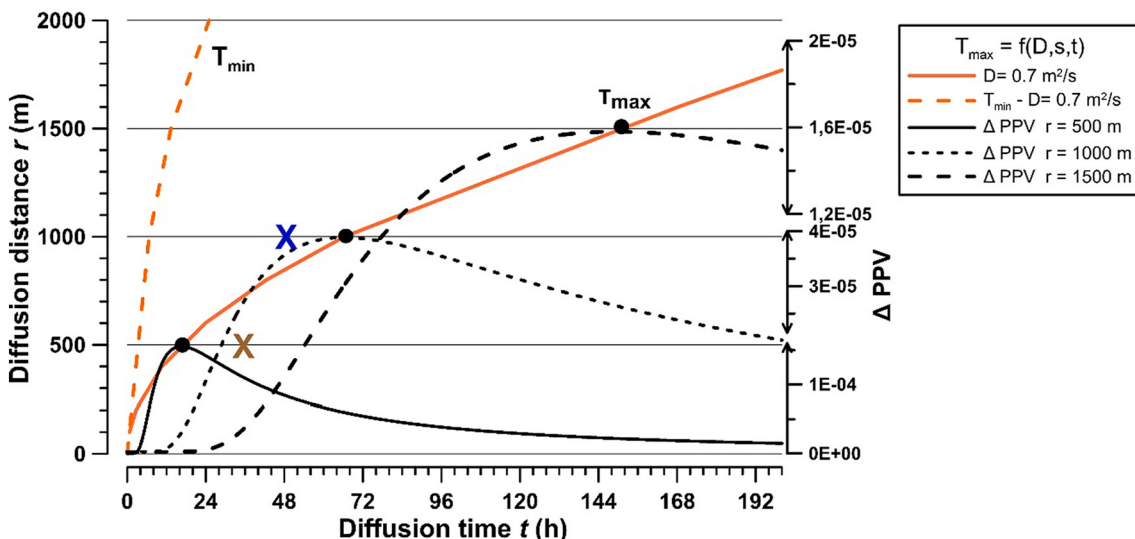
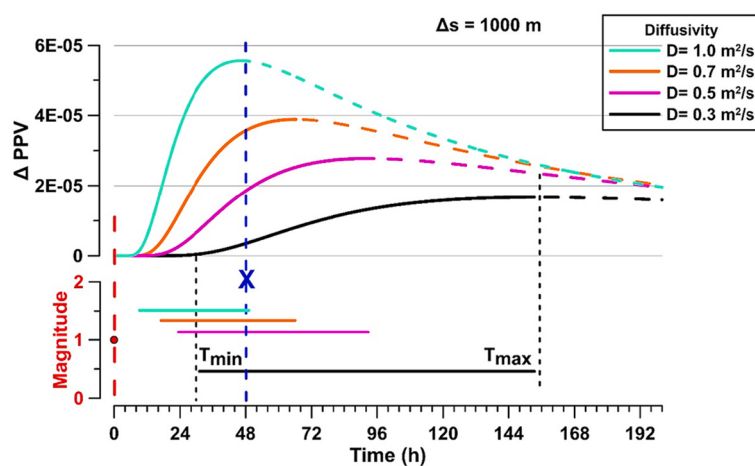


Fig. 5. Three pressure waves were calculated for three different diffusion distances ($r = 500 \text{ m}$, 1000 m and 1500 m) assuming an exemplary diffusivity of $D = 0.7 \text{ m}^2/\text{s}$ similar to the Figs. 3 and 4. The maxima of relative pore pressure increase ΔPPV are indicated by black points. The resultant orange line indicates the termination of the pore pressure increase also for other diffusion times and distances. T_{\min} was calculated from the onsets of pore pressure increase according to their diffusion periods and distances.

because it occurred before the maximum pressure increase T_{\max} approached this 'hypothetical' hypocentre.

This type of presentation, considering a wider range of diffusivities, identifies the periods of continuously pore pressure increase by SIPPPs at the respective diffusion distances. However, smaller diffusivities are always able to trigger these events, if the diffusion time is long enough, but with reduced pore pressure amplitude. As we show in the following steps, this graphical analysis of the spatiotemporal behaviour of pore pressure fronts was applied also to a wider range of diffusivities.

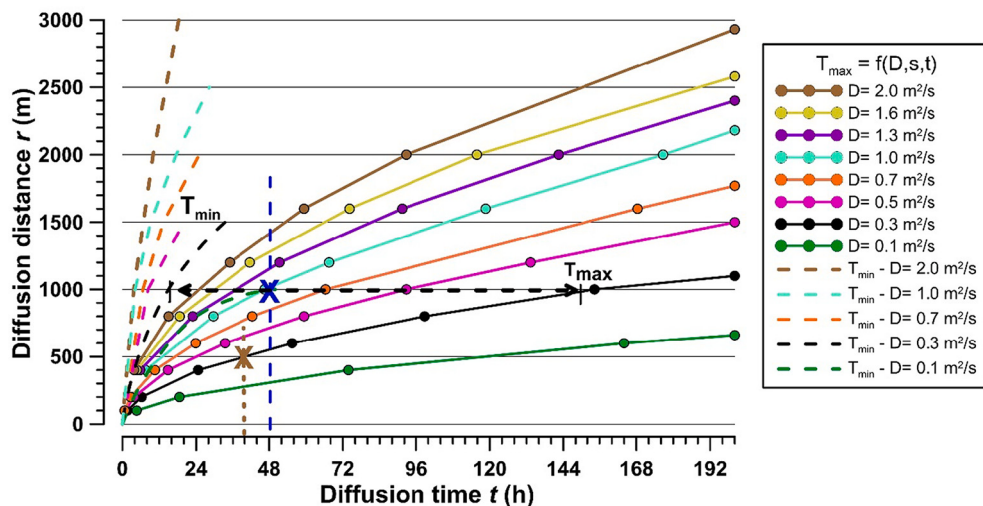
Fig. 6 demonstrates the graphical analysis with a wider range of diffusivities between 0.1 and $2.0 \text{ m}^2/\text{s}$ as well as the examples of the hypothetical seismic events in Figs. 3, 4 and 5 (stars). The figure shows the possible ranges of relevant diffusivities, e.g. the horizontal black dashed line with T_{\max} as parameter for the upper limit of the respective diffusivity ($D = 0.3 \text{ m}^2/\text{s}$) as in Fig. 4. The range of relevant diffusivities can be visually approximated in this r - t - D plot by the respective diffusion periods t of the SIPPPs to trigger the events, the diffusion distances r and the calculated points and connecting lines which indicate the maxima periods of pressure increase T_{\max} depending on the respective diffusivity. The relevant diffusivities are always equal or below the diffusivity corresponding to the upper limit of the respective T_{\max} . For example, the

blue star event could be triggered by SIPPPs if the diffusivity lies in the range of $D \leq 1.0 \text{ m}^2/\text{s}$ as previously shown in the Figs. 4 and 5. The amplitude of the SIPPPs would be the largest for $D = 1.0 \text{ m}^2/\text{s}$ but the trigger process could also be possible with smaller SIPPP amplitudes, e.g. with diffusivities of $D = 0.3 \text{ m}^2/\text{s}$. The proposed graphical analysis in Fig. 6 will be applied in the following evaluation of the 2008 earthquake swarm phases.

3. Results

The calculation of the maxima diffusion periods T_{\max} for different diffusivities and distances and their application in a r - t - D plot allow the approximation of the relevant diffusivity range for the real earthquake data. However, due to the numerous events of each swarm phase, we suggest a stepwise evaluation of the diffusion processes for each triggered phase P2 to P7 to improve the general understanding of the process.

The analysis of the pore fluid diffusion as a possible trigger of the earthquake swarm phases, such as during the 2008 swarm, needs some general assumptions to describe the possible trigger mechanism by SIPPPs:



could be only triggered by diffusivities of $D \leq 0.3 \text{ m}^2/\text{s}$ because of the relative long diffusion time of 40 h for a diffusion distance of only 500 m. (For interpretation of the references to colour in this figure legend, the reader is referred to the web version of this article.)

- A ‘general assumption’ is that all earthquakes of a swarm phase could possibly originate SIPPPs, which again are capable of triggering all events of the subsequent swarm phase. This simplification as a one-to-one trigger process is necessary because we do not know which seismic event induces the responsible SIPPP for the subsequent earthquakes. We assume that each of the events could be a responsible candidate. However, this is not the case in reality, because the relative distances between the single hypocentres vary significantly. Furthermore, the nearby induced SIPPPs would be of larger amplitude and probably faster, depending on the diffusion path and the diffusivity, independent of the pressure wave superposition, which cannot be handled here. However, this one-to-one approach can only be considered for the separated data sets of the six triggered swarm phases. For example: one, two or more of the 310 events of the subsequent swarm phase P2 could be triggered by SIPPPs induced by one of the 70 events of the swarm phase P1, which means we have to consider about 20.000 trigger options of the swarm phase P2 (see Fig. 8a).
- The onset of the first swarm phase P1 is not the target of this study, we consider only the trigger process of the subsequent swarm phases by the previous swarm phases (P1 trigger P2; P2 trigger P3, P3 trigger P4 etc.). We have also excluded that the respective swarm phase itself could be a self-triggered system of hydraulic trigger pulse generation. If this process exists, the diffusion times and distances will be in most cases probably shorter than the trigger process by the previous swarm phase. However, this will be a target of further studies.
- The events are triggered only during periods of pressure increase: the period before reaching T_{\max} at the hypocentre. A possible delay of the trigger effect, e.g. by stress corrosion or the influence of stress transfer (Hainzl and Ogata, 2005) is beyond the scope of this study.
- The proposed hypothesis suggests the theoretical assumption that each event of shear-compressive faulting induces a SIPPP, which could trigger the events of the subsequent swarm phase.
- We consider only a limited range of the diffusion distance (3000 m) and diffusion time (200 h) of the respective SIPPPs to describe the principal spatiotemporal behaviour of this possible trigger process. SIPPPs for longer distances and diffusion times can be calculated but we consider these limits as the most important ranges at the beginning of a swarm phase. Furthermore, the amplitudes of the SIPPPs fade away with longer distances and longer diffusion times. Our

Fig. 6. Graphical analysis of the calculated periods with increasing pore pressure on the base of the diffusion time t , the diffused distance r and with respect to the assumed diffusivity D . The parameter T_{\max} indicates for each presented diffusivity (coloured lines, see legend) the maximum duration of pressure increase for a certain diffusion distance r . T_{\min} marks the period up to the arrival of the pressure wave (dashed lines with the same colours in the legend). The figure reveals a simple approximation if the studied events (stars) could be triggered by SIPPPs and their possible diffusivity range, if the diffusion time and distance are known. The horizontal black dashed line, for example indicates the possible periods of pressure increase after a diffusion distance of approximately 1000 m according to their diffusivity of $D = 0.3 \text{ m}^2/\text{s}$. Higher diffusivities up to $1.0 \text{ m}^2/\text{s}$ are possible, as is also indicated in Fig. 4. These periods of pressure increase could be responsible for triggering the blue marked event. The brown star event

limits are an assumption of these first studies and based on results e.g. of the induced seismicity.

- We assume that all earthquakes of the respective phases contribute to the calculated SIPPP, despite the events of shear-tensile fracturing, which would reduce the calculated amplitude of the pressure wave. We assume that this reduction is negligible for a principal description of the spatiotemporal behaviour of the swarm phases. The comprehensive analysis of >4500 earthquakes during the earthquake swarms of the years 2008 to 2018 by Vavryčuk et al. (2021) shows that shear compressive fracturing is predominant.

The following two steps with different data sets will be applied for our analytic approach:

- #1 investigation of the three major earthquakes of each swarm phase;
- #2 analysis of the complete but separated trigger phases: P1–P2, P2–P3, P3–P4, P4–P5, P5–P6 and P6–P7.

3.1.1. Step 1: Investigation of the three major earthquakes of each swarm phase

Because of our formerly introduced ‘general assumptions’, we have strongly reduced the number of earthquakes in ‘Step 1’ to better understand the principal process. For our example, we have selected three major events of each phase (P1 to P6), because they could induce the largest pore pressure perturbations due to the collapse of the largest fracture radii and they could trigger, for example, the three largest events of the subsequent phase (P2 to P7). These events are listed in Table 1, according to the bulletin data provided by Vavryčuk (2021). Here we emphasize the advantage of the used seismic data and their location accuracy (Bouchala et al., 2013; Vavryčuk et al., 2021). This advantage improves the estimation of the diffusion distances to the events of the subsequent phases indicated in Fig. 7 by error bars.

We study the trigger processes of the phases: P1–P2, P2–P3, etc., exclusively using the three major earthquakes of each phases (Table 1). According to our proposed assumptions, each of these major events are potential candidates to induce a pressure front able to trigger each of the three strongest events in the subsequent swarm phases. This example of Step 1 reveals in total 54 possible trigger options according to their

Table 1

The three major events of each swarm phase P1 to P7, according to the bulletin in Vavryčuk (2021).

Date	Time	Longitude E	Latitude N	Depth (m)	local Magnitude	Swarm phase
06.10.2008	03:59:01	12,4534	50,2033	9686	2,0	P1
06.10.2008	04:01:20	12,4526	50,2032	9701	2,0	P1
06.10.2008	04:12:13	12,4553	50,2015	9540	2,0	P1
07.10.2008	19:20:18	12,4521	50,2049	9613	2,3	P2
08.10.2008	01:27:13	12,4548	50,2019	9657	2,4	P2
08.10.2008	02:32:08	12,4519	50,2080	9422	2,4	P2
09.10.2008	22:20:38	12,4509	50,2126	9129	3,6	P3
10.10.2008	11:18:41	12,4497	50,2175	9232	3,3	P3
10.10.2008	04:52:50	12,4500	50,2166	9247	2,8	P3
12.10.2008	07:19:57	12,4548	50,2044	8807	2,9	P4
12.10.2008	06:39:48	12,4517	50,2132	8998	2,8	P4
13.10.2008	01:42:47	12,4465	50,2134	10,213	2,9	P4
14.10.2008	04:01:36	12,4504	50,2137	9217	3,1	P5
14.10.2008	19:00:33	12,4539	50,2105	8280	3,8	P5
16.10.2008	10:48:22	12,4559	50,2116	7987	2,9	P5
21.10.2008	00:55:32	12,4488	50,2246	8529	2,7	P6
21.10.2008	01:39:39	12,4517	50,2175	8470	2,4	P6
21.10.2008	01:40:18	12,4517	50,2189	8412	2,4	P6
28.10.2008	08:27:35	12,4576	50,2089	7767	2,9	P7
28.10.2008	10:07:00	12,4576	50,2096	8001	2,9	P7
31.10.2008	03:17:44	12,4608	50,2144	7196	2,8	P7

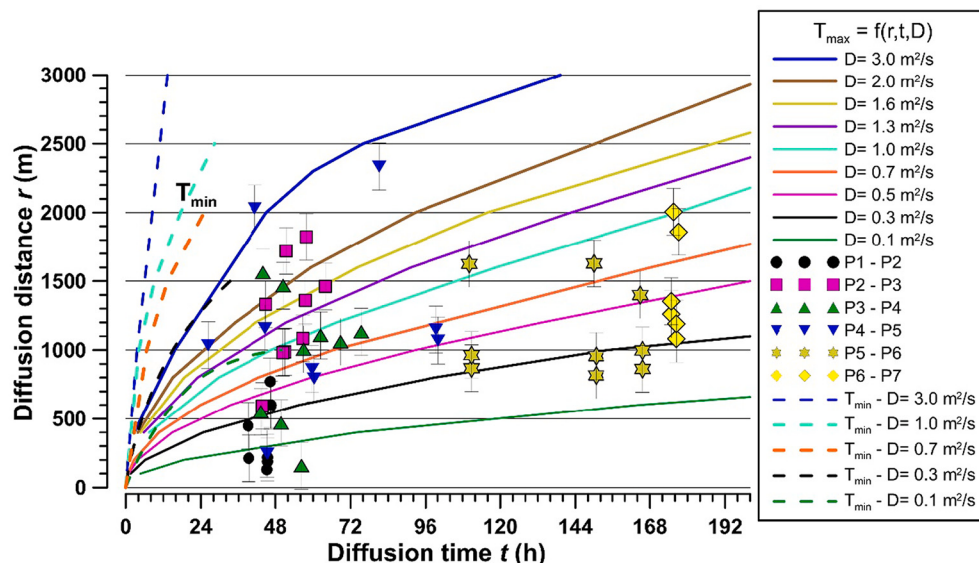


Fig. 7. The three major earthquakes of each phase (P2 to P7) could be triggered by SIPPPs induced by each of the three major earthquakes of the previous phase (P1 to P6, Table 1). These nine trigger options for each swarm phase (each of the 3 events of P1 could trigger each of P2, etc.) are indicated by the coloured signs for each trigger phase (see legend). The r - t - D plot suggests the possible diffusivity range for the selected SIPPPs according to their positions between the respective horizontal lines of T_{\min} and T_{\max} (see legend, not all T_{\min} are displayed for a better visual analysis, the missing lines are between the presented ones). For example, if all major earthquakes of the phase P3 (pink squares) are triggered by one of the respective SIPPPs of the three major earthquakes of phase P2, the diffusivity should be in the range of $D = 0.01$ to $2.5 \text{ m}^2/\text{s}$. The relative location errors of the hypocentres influence the diffusion distances and therefore are indicated by error bars. A few possible trigger options of the phases P1–P2, P2–P3 are not visible because of double printed points or a longer diffusion time than the presented time scale (P6–P7).

(For interpretation of the references to colour in this figure legend, the reader is referred to the web version of this article.)

necessary diffusion distances (direct path) and diffusion times (the difference between both focal times).

Fig. 7 shows the distribution of all possibly trigger options with their respective diffusion times and diffusion distances (phases P2 to P7) in an r - t - D plot according to Fig. 6. The periods of pore pressure increase between T_{\min} and T_{\max} with their specific diffusivities in the range of $D = 0.1$ to $3.0 \text{ m}^2/\text{s}$ are indicated in this figure. The largest diffusivity of the SIPPPs of the possibly triggered major earthquakes can be approximated from the horizontal position between the two enclosing diffusivity curves of T_{\max} . All further diffusivities of T_{\max} to the right of the maxima value are relevant. This visual analysis suggests the possible range of the real diffusivities for all assumed trigger processes. We are not able to resolve which diffusivity is the real value because of the unknown behaviour of the SIPPPs. However, the presented range of diffusivities ($D = 0.1$ to $3.0 \text{ m}^2/\text{s}$) fits the most part of the analysed range. We consider a minimum diffusivity of about $0.004 \text{ m}^2/\text{s}$ as the lowest limit

according to the data obtained from the KTB test site experiments at 5 km depth (Shapiro et al., 2006). The calculation of trigger options reveals much lower diffusivities but these values are not realistic because of the numerous other options with a faster diffusion of SIPPPs to trigger the same event.

The particular upper diffusivity ranges D_{\max} of Fig. 7 are: P1 – P2: $D_{\max} \leq 0.7 \text{ m}^2/\text{s}$; P2 – P3: $D_{\max} \leq 3.0 \text{ m}^2/\text{s}$; P3 – P4: $D_{\max} \leq 3.0 \text{ m}^2/\text{s}$; P4 – P5: $D_{\max} \leq 3.0 \text{ m}^2/\text{s}$; P5 – P6: $D_{\max} \leq 1.6 \text{ m}^2/\text{s}$; P6 – P7: $D_{\max} \leq 1.3 \text{ m}^2/\text{s}$.

3.1.2. Step 2: Analysis of the complete trigger phases P1 to P6

As the second step, we have estimated the distances and time differences between all events of the first swarm phase P1 and the possibly triggered second phase P2, and also for P2–P3, P4–P5, P5–P6 and P6–P7. The large number of possible triggered events of the respective subsequent phase due to the one-to-one approach increases the cloud of points

in the following r - t - D plots (Fig. 8 a-f). The result reflects, in principle, the previously observed distribution in Fig. 7, but with a wider range of D due to the larger number of widely distributed trigger options of each phase according to their respective diffusion distance, time and diffusivity. However, most of the assumed trigger processes are characterized by diffusivities below $10.0 \text{ m}^2/\text{s}$. We consider the increased diffusivity values above the range of $D > 10.0 \text{ m}^2/\text{s}$ as possible, e.g. along open fracture zones with high permeability, but this range would be exceptional (see discussion). The trigger process of phase P1-P2 gives no indications for such open fracture zones.

The numerous options due to the one-to-one analysis generates multiple trigger options of the same event. Further comprehensive studies of these uncertainties are necessary, which should include e.g. the influence of the magnitudes as important parameter for the SIPPP amplitude.

Taken all together, our analyses suggest for the first time an approximation of the effective diffusivity range for the Nový Kostel focal zone. Notably, the diffusivity range is restricted by an upper and probably also a lower limit, which is in the range of accepted data in the literature (see next section).

We also speculate that our general hypothesis could be relevant as a possible explanation of the swarm triggering process and their spatio-temporal behaviour, and it could even be a predominant process due to the prevailing shear compressive fracturing.

4. Discussion

Our study concerning the hypothesis of seismically induced pore pressure variations by the expulsion of fluids from compressive fracturing and their diffusion as possible trigger of the subsequent

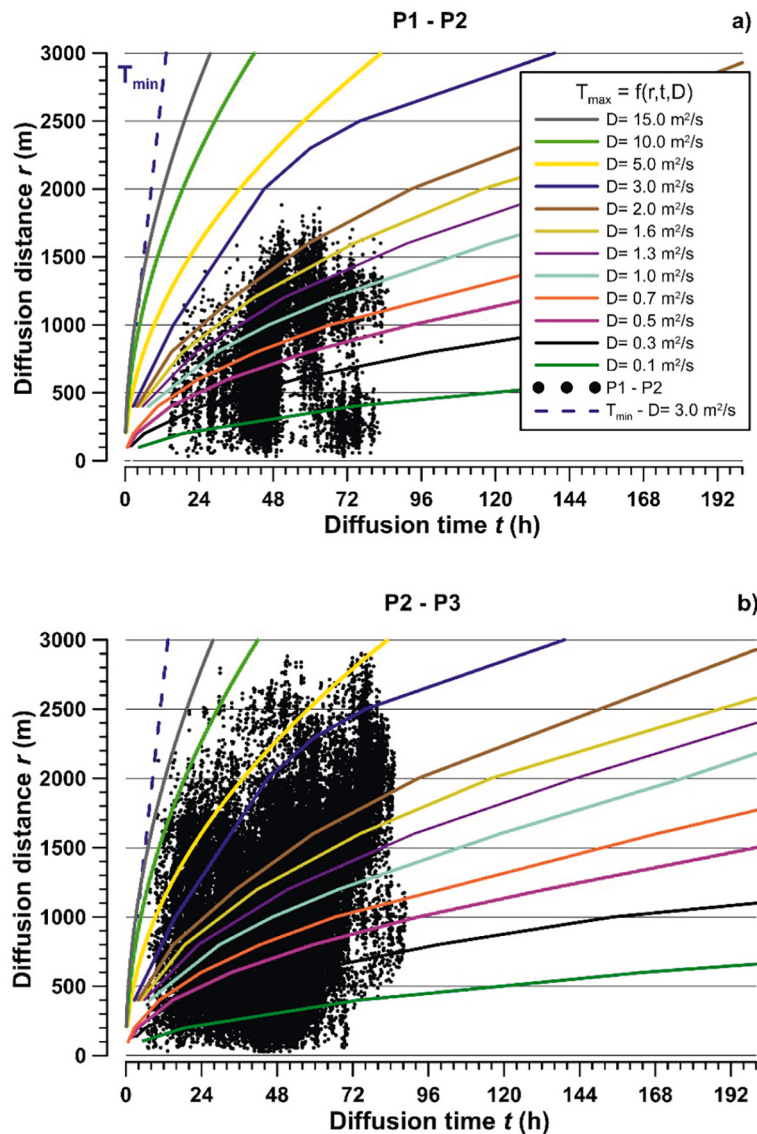


Fig. 8. a-f. The figures show the range of diffusivities for each trigger option (black points), which could be the trigger of the earthquakes of the respective subsequent swarm phases. The swarm phases (P2, P3, P4, P5, P6 and P7) could be triggered by SIPPPs induced by all earthquakes of the respective previous phases (P1, P2, P3 etc.), which is displayed in the separated trigger phases in the figures a to f. The legend of the diffusivity ranges in Fig. 8a is relevant for all figures. The r - t - D plots suggest the possible diffusivity range for the clouds of trigger options according to their positions to the respective T_{\max} of different diffusivities. For example, the analysis suggests for the first trigger process P1-P2 (Fig. 8a), diffusivities between 0.01 and $3.0 \text{ m}^2/\text{s}$ are necessary for the proposed trigger options. This result may not be unexpected but it is the first approximation that the SIPPP trigger process could exist and that the approximated diffusivities are in a typical range (see discussion). We have limited the presented data by the axis values because of the assumption that a presentation with larger axis values reflects an unrealistic picture of the trigger process: the SIPPPs decay with longer distances and diffusion periods and could probably not be strong enough for a trigger process.

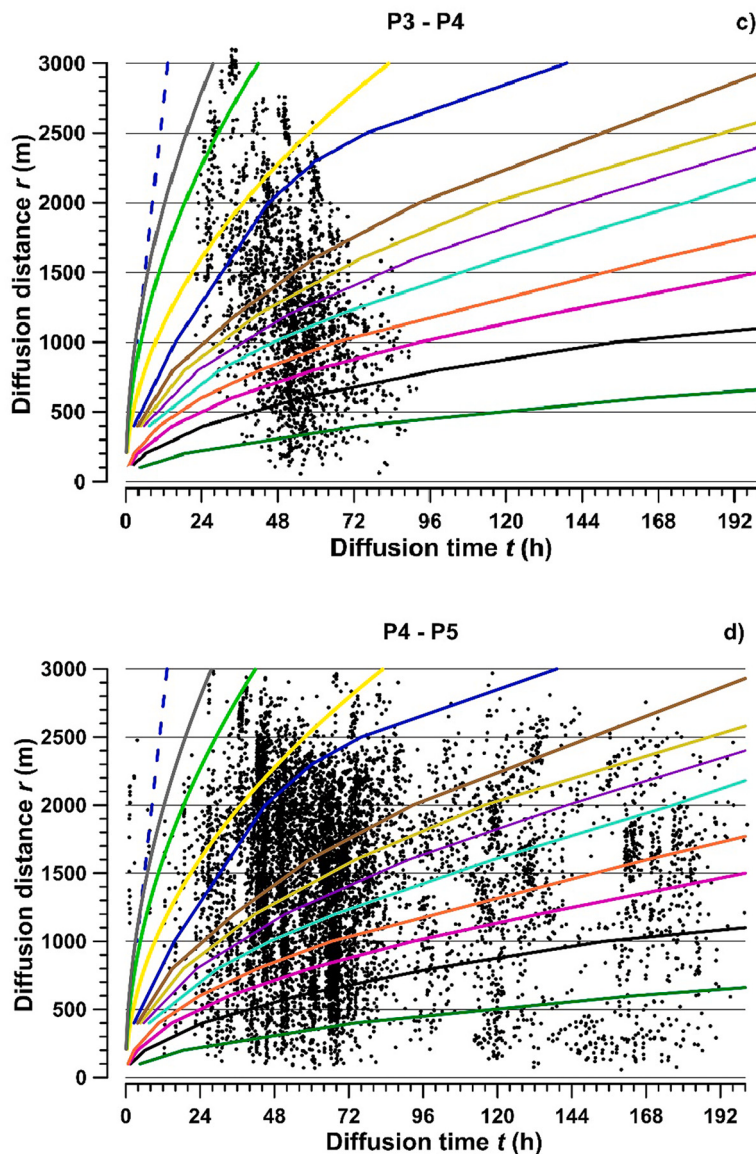


Fig. 8. (continued).

earthquake swarm phases could contribute to the understanding and explanation of the spatiotemporal behaviour of the earthquake swarm phenomena in the Nový Kostel focal zone.

The results show that after the initial earthquakes of a swarm the subsequent seismic events belonging to this first phase could be triggered by seismically induced hydraulic pore pressure pulses (SIPPPs). Their diffusion along an interconnected fracture system depends on their effective diffusivity, diffusion distance, and time; implying that the swarm itself could be a self-triggered system of hydraulic trigger pulse generations, until the critical stress is released and the respective swarm phases fade out. The diffusion of the pressure accumulation of all generated pressure pulses acts as a trigger front of the subsequent swarm phase and distributed microevents. Finally, it is possible that the cumulative effect of all factors, from the accumulated shear stress to the degradation of the rock matrix and the reduced frictional strength due to the SIPPPs could be the driving forces triggering the collapse of the weakened shear planes.

The weak point of this evaluation may be the missing information regarding the real diffusion distances. We can only assume the range of distances from the investigation of all events, which could have an influence on the pore pressure regime. The distances vary between

reactivated events very close to the released SIPPP up to 6 km for the far located swarm phases. We are unable to resolve which diffusion distance has a real trigger effect. We can only assume that the closer events probably induce the more active and relevant SIPPPs, since the shorter diffusion distances lead to a higher level of pore pressure perturbations and probably to shorter diffusion times. Additionally, the superposition of the SIPPPs in the hypocentres enlarges the fracture probability, but this process cannot be resolved. Therefore, we have proposed an analysis of all principal trigger processes with all earthquakes of the respective swarm phases in more or less all distances (up to 3 km).

Most part of the possible trigger mechanism by SIPPPs in the Figs. 7 and 8a-f reveal a majority for the diffusivity range between $D = 0.01$ and $3.0 \text{ m}^2/\text{s}$. SIPPPs which need diffusivities up to $15 \text{ m}^2/\text{s}$ to trigger events will be considered as exceptional because they need open fracture zones over long distances.

The analysed range of diffusivities is an important argument for our hypothesis. These diffusivities are in a realistic range for the studied area, which were analysed and confirmed in the following previous studies:

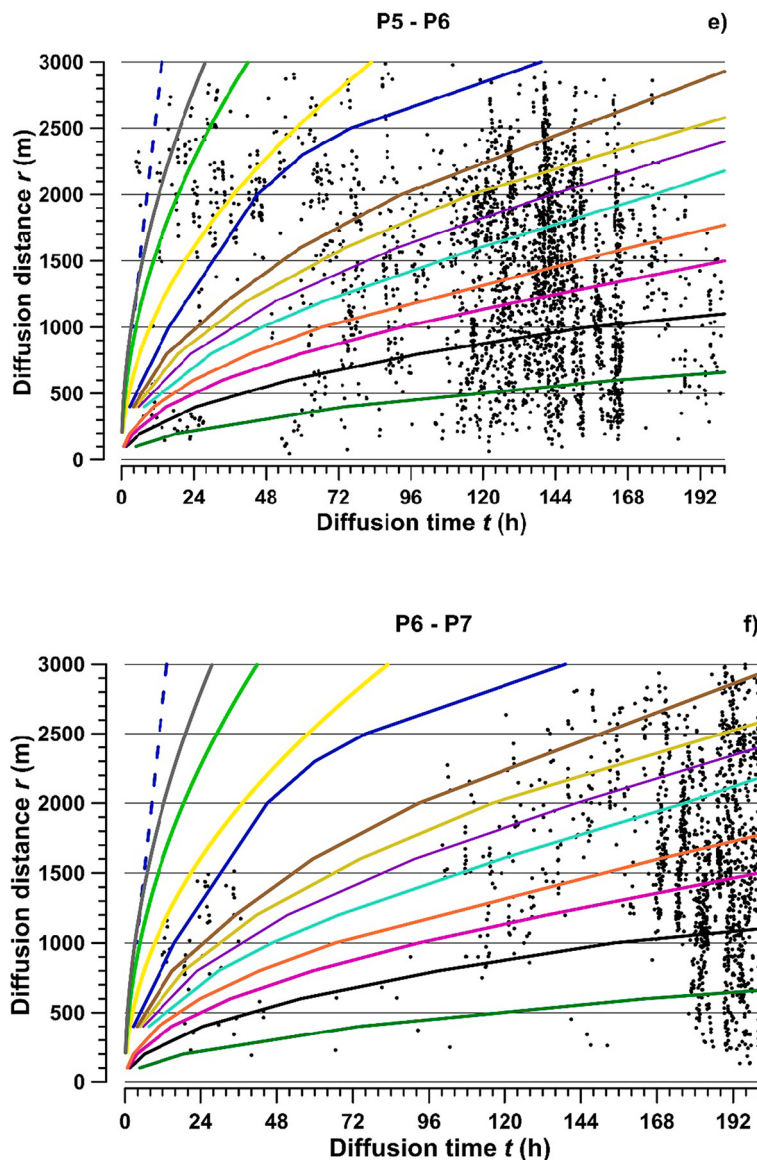


Fig. 8. (continued).

- An important hydraulic diffusivity value was obtained during the pressure tests at the KTB test site, which is located approximately 50 km southwest of our studied area. The hydraulic ‘communication’ between the KTB main borehole and the pilot borehole at 4 km depth during a long-term pressure test shows pressure signals after 1.5 days, which indicate a hydraulic diffusivity of $D = 0.12 \text{ m}^2/\text{s}$ (Kessels and Kück, 1995), a reliable value achieved in a similar geological basement characterized by crystalline and anisotropic rocks. Similar diffusivities were also analysed during fluid injection tests, which induced micro-seismicity at the KTB site with D -values of approximately 0.05 to $1.0 \text{ m}^2/\text{s}$ at 9 km depth and 0.004 to $0.01 \text{ m}^2/\text{s}$ at 5.4 km depth (Shapiro et al., 2006; Shapiro et al., 1997).
- The analysis of the swarm in the year 2000 reveals an expansion of the swarm earthquakes, which can be described by a diffuse propagation front of pore pressure wave according to formula (1) (Parotidis et al., 2005). The spatiotemporal distribution of the earthquakes follows a kind of parabolic envelope with the diffusivity as the describing parameter. The effective hydraulic diffusivity of the complete swarm was estimated as $D = 0.25 \text{ m}^2/\text{s}$. The analysis of the possible trigger process of the respective swarm phases reveals larger diffusivities, e.g., $D = \{0.3, 2, 3, 8, 6, 7, 10, 9\} \text{ m}^2/\text{s}$.
- Hainzl et al. (2012) suggest for the swarm in 2008 a separation of the up-dip and down-dip migration of the swarm phases with different diffusivities: $0.1 \text{ m}^2/\text{s}$ for down-dip and $0.3 \text{ m}^2/\text{s}$ for the up-dip diffusion. For the exceptional swarm of 2014, Hainzl et al. (2016) calculated a fast pore pressure diffusion with a hydraulic diffusivity of approximately $10 \text{ m}^2/\text{s}$. Bachura et al. (2021) described the opposite seismic expansion along two fault segments during the 2018 swarm as two possible pore pressure diffusion processes with hydraulic diffusivities of 1.9 and $3 \text{ m}^2/\text{s}$.
- Heinicke et al. (2018) estimated the hydraulic diffusivity for a hydroseismicity trigger process to be approximately 0.2 to $0.5 \text{ m}^2/\text{s}$ for the earthquake swarm activity at Nový Kostel between the years 1992 and 2016.
- Other investigations of induced seismicity caused by hydraulic injection experiments, e.g. the Fenton Hill and Soultz-sous-Forêts experiments, reveal hydraulic diffusivities of a similar range of approximately 0.17 and $0.05 \text{ m}^2/\text{s}$, respectively (Shapiro et al., 2002). The induced seismicity with a diffusivity of approximately $0.5 \text{ m}^2/\text{s}$ at the Castor gas reservoir (Cesca et al., 2021) confirm also the hydraulic diffusivity range of our results.

These examples from other investigations demonstrate a small range of probable hydraulic diffusivities between 0.1 and $10 \text{ m}^2/\text{s}$, also in the Nový Kostel focal zone. Our estimations vary between $D = 0.01$ and $3.0 \text{ m}^2/\text{s}$ and in some cases up to $15 \text{ m}^2/\text{s}$, depending on the swarm phases and the respective fracture zones and confirm the proposed range from the literature data.

Overall our results are consistent with the proposed hypothesis. Hence, we consider the SIPPP trigger process to be an option for an assumed spatiotemporal range of a diffusion distance of 3 km and a diffusion time of 200 days. It means that probably all events, which are too far or too late will not be triggered by SIPPPs.

Our analysis further suggests that the diffusion time to approach the hypocentres of the subsequent swarm phase could be an explanation for the spatiotemporal character of the earthquake swarm phenomena. This trigger delay is of relatively long-term character (hours, days, weeks) in comparison to the direct and fast trigger process due to stress diffusion. The SIPPP process would be able to explain this relatively slow behaviour depending on the fracture zones.

Our model is approximated for a 1-D pore pressure diffusion process. However, this pressure diffusion occurs in all three-dimensions according to the strike of the fractures, mostly N-S and E-W oriented, as well as vertical. For example, Bachura et al. (2021) observed such an opposite diffusion process along two fault segments of opposite orientation. However, our proposed hypothesis of the SIPPP and their diffusion is a proposal to explain in general the scattered occurrence of events with different temporal delays.

5. Conclusion

Our study shows that compressive fracturing as the prevailing focal mechanism during the earthquake swarms at Nový Kostel could be considered as a generation process of numerous pore fluid pressure pulses. These seismically induced pore pressure pulses (SIPPPs) could trigger the subsequent earthquakes in the active phase and trigger the onset of the next swarm phase subsequently to their respective diffusion. The visual analyses of $r-t$ - D plots reveal that a large number of events could be triggered by SIPPPs, which diffuse within an acceptable range of effective diffusivities ($D = 0.01\text{--}3.0 \text{ m}^2/\text{s}$). Higher diffusivities up to $15 \text{ m}^2/\text{s}$ are an exception for open fractures in the upper crust. The lack of concrete diffusion distances can be solved by an analysis of the complete range of all possible diffusion distances in a one-to-one approach. The proposed visual analysis indicates the possible periods of trigger processes by a SIPPP for a wide range of diffusion times and distances.

The diffusion of the pressure pulses in a 3D pore space and fracture zone would be an explanation of the temporal and spatial distribution of the subsequent swarm earthquakes and their corresponding swarm phases according to the respective effective hydraulic diffusivities. Attenuation of the pressure pulses and stress release lets the swarm fade out.

The results obtained for this intraplate earthquake swarm area could probably also be adapted to other earthquake swarm regions worldwide if shear compressive faulting is the prevailing focal mechanism.

Data availability

The data underlying this article are available on the web page of the WEst Bohemian local seismic NETwork (WEBNET, 2021) and in the articles and in its online supplementary material of Vavryčuk and Hrubcová (2017), Vavryčuk et al. (2021) and the Medeley Data in Vavryčuk (2021).

CRediT authorship contribution statement

Jens Heinicke: Conceptualization, Data curation, Investigation, Methodology, Software, Writing – original draft. **Thomas Braun:**

Conceptualization, Investigation, Methodology, Writing – original draft. **Catherine Alexandrakis-Zieger:** Conceptualization, Data curation, Methodology, Writing – original draft. **Stefan Buske:** Conceptualization, Methodology, Supervision, Project administration.

Declaration of Competing Interest

None.

Acknowledgements

We acknowledge support and providing of seismological data by the West Bohemia Seismic Network WEBNET. The authors are grateful to P. Talwani for fruitful discussions and helpful comments. The authors would like to thank very much the anonymous reviewers and the editor Prof. A. Ferreira for the very constructive reviews and comments. This work was supported by the German Research Foundation (DFG) [grant HE2177/16-2].

References

- Babuška, V., Růžek, B., Dolejš, D., 2016. Origin of earthquake swarms in the western Bohemian Massif: is the mantle CO₂ degassing, followed by the Cheb Basin subsidence, an essential driving force? *Tectonophysics* 668–669, 42–51. <https://doi.org/10.1016/j.tecto.2015.12.008>.
- Bachura, M., Fischer, T., Doubravová, J., Horálek, J., 2021. From earthquake swarm to a main shock-aftershocks: the 2018 activity in West Bohemia/Vogtland. *Geophys. J. Int.* 224, 1835–1848. <https://doi.org/10.1093/gji/ggaa523>.
- Bouchala, F., Vavryčuk, V., Fischer, T., 2013. Accuracy of the master-event and double-difference locations: synthetic tests and application to seismicity in West Bohemia, Czech Republic. *J. Seismol.* 17, 841–859. <https://doi.org/10.1007/s10950-013-9357-4>.
- Bräuer, K., Kämpf, H., Koch, U., Niedermann, S., Strauch, G., 2007. Seismically induced changes of the fluid signature detected by a multi-isotope approach (He, CO₂, CH₄, N₂) at the Wettingquelle, Bad Brambach (central Europe). *J. Geophys. Res. Solid Earth* 112. <https://doi.org/10.1029/2006jb004404>.
- Bräuer, K., Kämpf, H., Niedermann, S., Strauch, G., Tesař, J., 2008. Natural laboratory NW Bohemia: comprehensive fluid studies between 1992 and 2005 used to trace geodynamic processes. *Geochem. Geophys. Geosyst.* 9 <https://doi.org/10.1029/2007gc001921>.
- Bräuer, K., Kämpf, H., Strauch, G., 2014. Seismically triggered anomalies in the isotope signatures of mantle-derived gases detected at degassing sites along two neighboring faults in NW Bohemia, central Europe. *J. Geophys. Res. Solid Earth* 119. <https://doi.org/10.1002/2014jb011044>.
- Cesca, S., Stich, D., Grigoli, F., Yuan, A., López-Comino, J.Á., Niemz, P., Blanch, E., Dahm, T., Ellsworth, W.L., 2021. Seismicity at the Castor gas reservoir driven by pore pressure diffusion and asperities loading. *Nat. Commun.* 12, 4783. <https://doi.org/10.1038/s41467-021-24949-1>.
- Cháb, J., Stránský, Z., Eliáš, M., 2007. *Geologická mapa České republiky*, 1st ed. Česká Geolog. Služba, Praha.
- Chen, L., Talwani, P., 2001. Renewed seismicity near Monticello Reservoir, South Carolina, 1996–1999. *Bull. Seismol. Soc. Am.* 91, 94–101. <https://doi.org/10.1785/01200000083>.
- Costain, J.K., 2008. Intraplate seismicity, hydroseismicity, and predictions in hindsight. *Seismol. Res. Lett.* 79, 578–589. <https://doi.org/10.1785/gssrl.79.4.578>.
- Dahm, T., Fischer, T., Hainzl, S., 2008. Mechanical intrusion models and their implications for the possibility of magma-driven swarms in NW Bohemia Region. *Stud. Geophys. Geod.* 52, 529–548. <https://doi.org/10.1007/s11200-008-0036-9>.
- Dahm, T., Heimann, S., Funke, S., Wendt, S., Rappitschler, I., Bindl, D., Plenefisch, T., Cotton, F., 2018. Seismicity in the block mountains between Halle and Leipzig, Central Germany: centroid moment tensors, ground motion simulation, and felt intensities of two $M \approx 3$ earthquakes in 2015 and 2017. *J. Seismol.* 22, 985–1003. <https://doi.org/10.1007/s10950-018-9746-9>.
- Durá-Gómez, I., Talwani, P., 2010. Hydromechanics of the Koyna–Warna Region, India. *Pure Appl. Geophys.* 167, 183–213. <https://doi.org/10.1007/s00024-009-0012-5>.
- Emmert, U.V., Horstig, G., Stettner, G., 2007. General Geological Map of the Federal Republic of Germany – CC 6334 Bayreuth: GÜK200 - CC 6334 Bayreuth. Bundesanstalt für Geowissenschaften und Rohstoffe, Hannover.
- Eyre, T.S., Zecevic, M., Salvage, R.O., Eaton, D.W., 2020. A long-lived swarm of hydraulic fracturing-induced seismicity provides evidence for aseismic slip. *Bull. Seismol. Soc. Am.* 110, 2205–2215. <https://doi.org/10.1785/0120200107>.
- Fischer, T., Horálek, J., 2005. Slip-generated patterns of swarm microearthquakes from West Bohemia/Vogtland (central Europe): evidence of their triggering mechanism? *J. Geophys. Res. Solid Earth* 110. <https://doi.org/10.1029/2004jb003363>.
- Fischer, T., Horálek, J., Michálek, J., Boušková, A., 2010. The 2008 West Bohemia earthquake swarm in the light of the WEBNET network. *J. Seismol.* 14, 665–682. <https://doi.org/10.1007/s10950-010-9189-4>.
- Fischer, T., Horálek, J., Hrubcová, P., Vavryčuk, V., Bräuer, K., Kämpf, H., 2014. Intratidal earthquake swarms in West Bohemia and Vogtland: a review. *Tectonophysics* 611, 1–27. <https://doi.org/10.1016/j.tecto.2013.11.001>.

- Fischer, T., Matyska, C., Heinicke, J., 2017. Earthquake-enhanced permeability - evidence from carbon dioxide release following the ML 3.5 earthquake in West Bohemia. *Earth Planet. Sci. Lett.* 460, 60–67. <https://doi.org/10.1016/j.epsl.2016.12.001>.
- Foulger, G., Julian, B., Hill, D., Pitt, A., Malin, P., Shalev, E., 2004. Non-double-couple microearthquakes at Long Valley caldera, California, provide evidence for hydraulic fracturing. *J. Volcanol. Geotherm. Res.* 132, 45–71. [https://doi.org/10.1016/S0377-0273\(03\)00420-7](https://doi.org/10.1016/S0377-0273(03)00420-7).
- Gautheron, C., Moreira, M., Allègre, C., 2005. He, Ne and Ar composition of the European lithospheric mantle. *Chem. Geol.* 217, 97–112. <https://doi.org/10.1016/j.chemgeo.2004.12.009>.
- Hainzl, S., Fischer, T., 2002. Indications for a successively triggered rupture growth underlying the 2000 earthquake swarm in Vogtland/NW Bohemia. *J. Geophys. Res.* 107, ESE 5-1–ESE 5-9. <https://doi.org/10.1029/2002jb001865>.
- Hainzl, S., Ogata, Y., 2005. Detecting fluid signals in seismicity data through statistical earthquake modeling. *J. Geophys. Res. Solid Earth* 110. <https://doi.org/10.1029/2004jb003247>.
- Hainzl, S., Fischer, T., Dahm, T., 2012. Seismicity-based estimation of the driving fluid pressure in the case of swarm activity in Western Bohemia. *Geophys. J. Int.* 191, 271–281. <https://doi.org/10.1111/j.1365-246X.2012.05610.x>.
- Hainzl, S., Fischer, T., Čermáková, H., Bachura, M., Vlček, J., 2016. Aftershocks triggered by fluid intrusion: evidence for the aftershock sequence occurred 2014 in West Bohemia/Vogtland. *J. Geophys. Res. Solid Earth* 121, 2575–2590. <https://doi.org/10.1002/2015JB012582>.
- Heidbach, O., Rajabi, M., Cui, X., Fuchs, K., Müller, B., Reinecker, J., Reiter, K., Tingay, M., Wenzel, F., Xie, F., Ziegler, M.O., Zoback, M.-L., Zoback, M., 2018. The World Stress Map database release 2016: crustal stress pattern across scales. *Tectonophysics* 744, 484–498. <https://doi.org/10.1016/j.tecto.2018.07.007>.
- Heinicke, J., Fischer, T., Gaupp, R., Götz, J., Koch, U., Konietzky, H., Stanek, K.P., 2009. Hydrothermal alteration as a trigger mechanism for earthquake swarms: the Vogtland/NW Bohemia region as a case study. *Geophys. J. Int.* 178, 1–13. <https://doi.org/10.1111/j.1365-246X.2009.04138.x>.
- Heinicke, J., Woith, H., Alexandrakis, C., Buske, S., Telesca, L., 2018. Can hydroseismicity explain recurring earthquake swarms in NW-Bohemia? *Geophys. J. Int.* 212, 211–228.
- Heinicke, J., Stephan, T., Alexandrakis, C., Gaupp, R., Buske, S., 2019. Alteration as possible cause for transition from brittle failure to aseismic slip: the case of the NW-Bohemia / Vogtland earthquake swarm region. *J. Geodyn.* 124, 79–92. <https://doi.org/10.1016/j.jog.2019.01.010>.
- Heinze, T., Hamidi, S., Galvan, B., Miller, S.A., 2017. Numerical simulation of the 2008 West-Bohemian earthquake swarm. *Tectonophysics* 694, 436–443. <https://doi.org/10.1016/j.tecto.2016.11.028>.
- Horálek, J., Fischer, T., 2008. Role of crustal fluids in triggering the West Bohemia/Vogtland earthquake swarms: just what we know (a review). *Stud. Geophys. Geod.* 52, 455–478. <https://doi.org/10.1007/s11200-008-0032-0>.
- Horálek, J., Šílený, J., 2013. Source mechanisms of the 2000 earthquake swarm in the West Bohemia/Vogtland region (Central Europe). *Geophys. J. Int.* 194, 979–999. <https://doi.org/10.1093/gji/ggt138>.
- Hořík, K., Tischendorf, G., Berger, H.J., 1981. *Geologische Karte Erzgebirge / Vogtland. In: Sächsisches Landesamt für Umwelt und Geologie.*
- Julian, B.R., Miller, A.D., Foulger, G.R., 1998. Non-double-couple earthquakes 1. Theory. *Rev. Geophys.* 36, 525–549. <https://doi.org/10.1029/98RG00716>.
- Kessels, W., Kück, J., 1995. Hydraulic communication in crystalline rock between the two boreholes of the continental deep drilling project in Germany. *Int. J. Rock Mech. Mining Sci. Geomech. Abstr.* 32, 37–47. [https://doi.org/10.1016/0148-9062\(94\)00017-W](https://doi.org/10.1016/0148-9062(94)00017-W).
- Kolář, P., Růžek, B., Boušková, A., Horálek, J., 2011. Visualization of the fault slip connected with the West Bohemia earthquake swarms. *Acta Geodyn. Geomater.* 8, 169–187.
- Michálek, J., Fischer, T., 2013. Source parameters of the swarm earthquakes in West Bohemia/Vogtland. *Geophys. J. Int.* 195, 1196–1210. <https://doi.org/10.1093/gji/ggt286>.
- Parotidis, M., Rothert, E., Shapiro, S.A., 2003. Pore-pressure diffusion: a possible triggering mechanism for the earthquake swarms 2000 in Vogtland/NW-Bohemia, central Europe. *Geophys. Res. Lett.* 30 <https://doi.org/10.1029/2003gl018110>.
- Parotidis, M., Shapiro, S.A., Rothert, E., 2005. Evidence for triggering of the Vogtland swarms 2000 by pore pressure diffusion. *J. Geophys. Res. Solid Earth* 110. <https://doi.org/10.1029/2004jb003267>.
- Shapiro, S.A., 2015. *Fluid-Induced Seismicity*. Cambridge University Press, Cambridge.
- Shapiro, S.A., Huenges, E., Borm, G., 1997. Estimating the crust permeability from fluid-injection-induced seismic emission at the KTB site. *Geophys. J. Int.* 131, F15–F18. <https://doi.org/10.1111/j.1365-246X.1997.tb01215.x>.
- Shapiro, S.A., Rothert, E., Rath, V., Rindschwendner, J., 2002. Characterization of fluid transport properties of reservoirs using induced microseismicity. *Geophysics* 67, 212–220. <https://doi.org/10.1190/1.1451597>.
- Shapiro, S.A., Kummerow, J., Dinske, C., Asch, G., Rothert, E., Erzinger, J., Kümpel, H.J., Kind, R., 2006. Fluid induced seismicity guided by a continental fault: injection experiment of 2004/2005 at the German Deep Drilling Site (KTB). *Geophys. Res. Lett.* 33 <https://doi.org/10.1029/2005gl024659>.
- Shelly, D.R., Moran, S.C., Thelen, W.A., 2013. Evidence for fluid-triggered slip in the 2009 Mount Rainier, Washington earthquake swarm. *Geophys. Res. Lett.* 40, 1506–1512. <https://doi.org/10.1002/grl.50354>.
- Stober, I., Bucher, K., 2015. Hydraulic conductivity of fractured upper crust: insights from hydraulic tests in boreholes and fluid-rock interaction in crystalline basement rocks. *Geofluids* 15, 161–178. <https://doi.org/10.1111/gfl.12104>.
- Talwani, P., Chen, L., Gahalaut, K., 2007. Seismogenic permeability, ks. *J. Geophys. Res.* 112 <https://doi.org/10.1029/2006JB004665>.
- Vavryčuk, V., 1993. Crustal anisotropy from local observations of shear-wave splitting in West Bohemia, Czech Republic. *Bull. Seismol. Soc. Am.* 83, 1420–1441.
- Vavryčuk, V., 2002. Non-double-couple earthquakes of 1997 January in West Bohemia, Czech Republic: evidence of tensile faulting. *Geophys. J. Int.* 149, 364–373. <https://doi.org/10.1046/j.1365-246X.2002.01654.x>.
- Vavryčuk, V., 2005. Focal mechanisms in anisotropic media. *Geophys. J. Int.* 161, 334–346. <https://doi.org/10.1111/j.1365-246X.2005.02585.x>.
- Vavryčuk, V., 2011. Tensile earthquakes: theory, modeling, and inversion. *J. Geophys. Res. Solid Earth* 116. <https://doi.org/10.1029/2011JB008770>.
- Vavryčuk, V., 2021. WEBNET Data 2008–2018: Mendeley Data. <https://doi.org/10.17632/4swk36hbvz.1>.
- Vavryčuk, V., Adamová, P., 2019. Non-double-couple moment tensors of earthquakes calculated using empirical green's functions. *Seismol. Res. Lett.* 91, 390–398. <https://doi.org/10.1785/0220190154>.
- Vavryčuk, V., Hrubcová, P., 2017. Seismological evidence of fault weakening due to erosion by fluids from observations of intraplate earthquake swarms. *J. Geophys. Res. Solid Earth* 122, 3701–3718. <https://doi.org/10.1002/2017jb013958>.
- Vavryčuk, V., Bohnhoff, M., Jechumtálková, Z., Kolář, P., Šílený, J., 2008. Non-double-couple mechanisms of microearthquakes induced during the 2000 injection experiment at the KTB site, Germany: a result of tensile faulting or anisotropy of a rock? *Tectonophysics* 456, 74–93. <https://doi.org/10.1016/j.tecto.2007.08.019>.
- Vavryčuk, V., Bouchala, F., Fischer, T., 2013. High-resolution fault image from accurate locations and focal mechanisms of the 2008 swarm earthquakes in West Bohemia, Czech Republic. *Tectonophysics* 590, 189–195. <https://doi.org/10.1016/j.tecto.2013.01.025>.
- Vavryčuk, V., Adamová, P., Doubravová, J., Ren, Y., 2021. Mapping stress and fluids on faults by nonshear earthquakes. *J. Geophys. Res. Solid Earth* 126. <https://doi.org/10.1029/2020JB021287>.
- Vidale, J.E., Shearer, P.M., 2006. A survey of 71 earthquake bursts across southern California: exploring the role of pore fluid pressure fluctuations and aseismic slip as drivers. *J. Geophys. Res. Solid Earth* 111. <https://doi.org/10.1029/2005jb004034>.
- WEBNET, 2021. West Bohemia Local Seismic Network. Institute of Geophysics, Academy of Sciences of the Czech Republic. <https://doi.org/10.7914/SN/WB>.
- Weise, S.M., Bräuer, K., Kämpf, H., Strauch, G., Koch, U., 2001. Transport of mantle volatiles through the crust traced by seismically released fluids: a natural experiment in the earthquake swarm area Vogtland/NW Bohemia, Central Europe. *Tectonophysics* 336, 137–150.
- Wintsch, R.P., Christoffersen, R., Kronenberg, A.K., 1995. Fluid-rock reaction weakening of fault zones. *J. Geophys. Res.* 100, 13021–13032. <https://doi.org/10.1029/94JB02622>.